

Study of e^+e^- annihilation at low energies

V.P. Druzhinin

Budker Institute of Nuclear Physics, Novosibirsk 630090, Russia

October 29, 2018

Abstract

The recent results of the CMD-2, SND, KLOE, and BABAR experiments on e^+e^- annihilation into hadrons at low energies are reviewed.

1 Introduction

The e^+e^- annihilation at low energies, below 3 GeV, is the main source of information on the properties of the light vector mesons (ρ , ω , ϕ) and their excited states. Other important application of the e^+e^- annihilation is calculation of the hadronic contribution into the anomalous magnetic moment of muon a_μ^{had} and the running electromagnetic constant. The difference between the measured value of a_μ [1] and recent Standard model calculations [2, 3, 4] varies from 3.2 to 3.4 sigma. Currently the hadronic leading-order contribution into a_μ is dominant source of uncertainty of the Standard model a_μ prediction. It is evaluated using experimental data on e^+e^- annihilation via dispersion integral

$$a_\mu^{\text{had}} = \int_{4m_\pi^2}^{\infty} ds K(s) R(s),$$

where $R(s)$ is the ratio of the total cross section of the e^+e^- annihilation into hadrons to the $e^+e^- \rightarrow \mu^+\mu^-$ cross section, and $K(s)$ is the kernel function decreasing monotonically as approximately $1/s^2$. Due to such s -dependence of $K(s)$ the main contribution into a_μ^{had} comes from the low energy region. Table 1 shows the contributions of the different e^+e^- center-of-mass (c.m.) energy

regions and the different processes into the a_μ^{had} [2]. It is seen that the dominant contribution both into the a_μ^{had} value and into its uncertainty comes from the energy region below 1.8 GeV and from the process $e^+e^- \rightarrow \pi^+\pi^-$.

The R energy dependence [5] for energies below 3 GeV is shown in Fig.1. The arrows indicate the energy regions covered by the present and future experiments contributing into the R measurement at low energies. In the resonant energy region, below 2 GeV, the total cross section is obtained by summing the exclusive cross sections for different hadronic final modes. For higher energies the inclusive approach is used. For $E < 1.4$ GeV, the most full and accurate data were obtained in CMD-2 and SND experiments at VEPP-2M. The VEPP-2M e^+e^- collider finished to work in 2000. Now this machine is substituted by the new collider VEPP-2000 with maximal energy of 2 GeV. The experiments at VEPP-2000 with SND and CMD-3 detectors will start in 2008. The most accurate measurement of the total hadronic cross section in the 2–3 GeV range was performed by BES detector [6]. New measurement in this energy range is planned at VEPP-4 e^+e^- collider with KEDR detector.

The relatively new initial state radiation (ISR) or radiative return technique is used for measurements of exclusive hadronic cross sections at high luminosity e^+e^- factories. The Born cross section for the ISR process $e^+e^- \rightarrow f + \gamma$ (Fig.2), where f is hadronic system, integrated over the hadron momenta,

Table 1: The contributions of different final states to a_μ^{had} , given in units of 10^{-10} .

Modes	a_μ^{had}
$\pi^+\pi^-$	$504.6 \pm 3.1 \pm 1.0_{\text{rad}}$
4π	$29.9 \pm 1.4 \pm 0.2_{\text{rad}}$
ω	$38.0 \pm 1.0 \pm 0.3_{\text{rad}}$
ϕ	$35.7 \pm 0.8 \pm 0.2_{\text{rad}}$
other, $E < 1.8$ GeV	$24.3 \pm 1.3 \pm 0.2_{\text{rad}}$
$E > 1.8$ GeV	$58.4 \pm 0.5 \pm 0.7_{\text{QCD}}$
sum	$690.8 \pm 3.9 \pm 1.9_{\text{rad}} \pm 0.7_{\text{QCD}}$

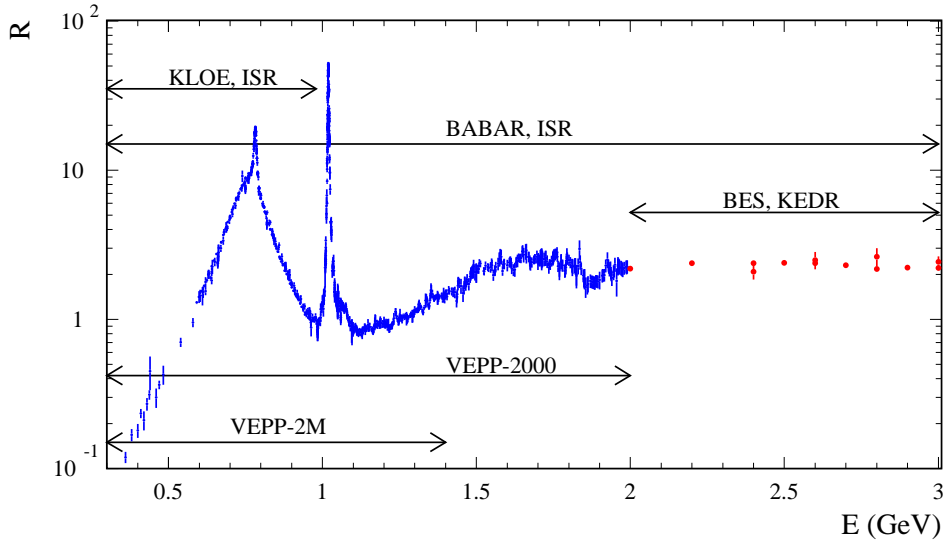


Figure 1: The R dependence on e^+e^- center of mass energy. The arrows indicate the energy regions covered by the present and future experiments contributing into the R measurement at low energies.

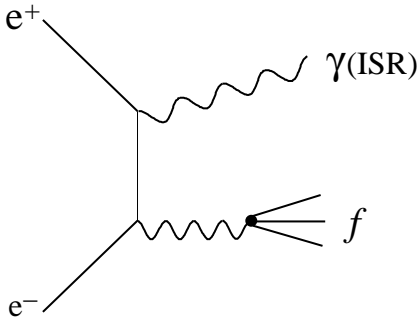


Figure 2: The diagram of the $e^+e^- \rightarrow f\gamma$ process, where f is hadronic system.

is given by

$$\frac{d\sigma_{e^+e^- \rightarrow f\gamma}(m)}{dm d\cos\theta_\gamma} = \frac{2m}{s} W(s, x, \theta_\gamma) \sigma_f(m),$$

where \sqrt{s} is the e^+e^- c.m. energy, m is the invariant mass of the hadronic system, $\sigma_f(m)$ is the cross section for $e^+e^- \rightarrow f$ reaction, $x \equiv E_\gamma/\sqrt{s} = 1 - m^2/s$, E_γ and θ_γ are the ISR photon energy and polar angle, respectively, in the e^+e^- c.m. frame. The function $W(s, x, \theta_\gamma)$ [7] describes the probability of the ISR photon emission. The ISR photon is predominantly emitted along beam axis. Two approaches are used for ISR measurements, with and without detection of the photon. The approach with undetected photon, in principle, provides higher detection efficiency for ISR events, but this efficiency strongly depends on the invariant mass of the hadronic system. The finite detector acceptance does not allow to use this approach for measurements in the near-threshold mass region. The approach with detected photon ($30^\circ < \theta_\gamma < 150^\circ$) utilizes only about 10% of ISR events but provides the weak dependence of the detection efficiency on the mass of the hadronic system and its internal substructure. The undetected approach is used by KLOE detector at ϕ -factory to measure the $e^+e^- \rightarrow \pi^+\pi^-$ cross section. The approach with detected photon is used by BABAR at B -factory ($\sqrt{s} = 10.6$ GeV).

2 VEPP-2M results

The CMD-2 and SND detectors took data at the VEPP-2M e^+e^- collider during 1995–2000. The total integrated luminosity collected by the two detectors in the energy range 0.36–1.4 GeV is about 60 pb^{-1} . All major hadronic cross sections were measured. The latest published results are measurements of the $e^+e^- \rightarrow K^+K^-$ [8] and $e^+e^- \rightarrow \eta\gamma$ [9] cross sections at SND. Analyses of some important modes are in progress. In particular, new results on $e^+e^- \rightarrow 3\pi$, $\pi^+\pi^-2\pi^0$, K^+K^- are expected from CMD-2, and $e^+e^- \rightarrow 2\pi$ for $E > 1$ GeV and $e^+e^- \rightarrow \pi^0\gamma$ from SND. The relative contributions of different processes measured at VEPP-2M and achieved statistical accuracy of the cross-section measurements are demonstrated in Fig. 3.

The most important process for calculation of the a_μ^{had} is $e^+e^- \rightarrow 2\pi$. At CMD-2 this process was measured in the energy range from 0.37 GeV up to 1.38 GeV [10, 11, 12, 13]. The systematic uncertainty of the CMD-2 measurement is 0.6–0.8% for $E < 1$ GeV. For energies above 1 GeV it varies from 1.2% to 4.2%. The SND measured the $e^+e^- \rightarrow 2\pi$ cross section in the energy range 0.4–1.0 GeV with the systematic uncertainty of 1.3% [14]. There is also SND measurement in the ϕ -meson vicinity [14]. The CMD-2 and SND results are compared in Fig. 4. The data of two detectors are in good agreement.

3 KLOE results

High statistics measurement of the $e^+e^- \rightarrow \pi^+\pi^-$ cross section in the energy range 0.59–0.97 GeV was performed by KLOE [16] using ISR technique on data collected in 2001. The ISR photon was required to be emitted with $\theta_\gamma < 15^\circ$ and $\theta_\gamma > 165^\circ$. This requirement minimizes the contribution of the final state radiation which is significant at $\sqrt{s} = 1.02$ GeV. The 2π contribution into a_μ^{had} evaluated by KLOE from the measured $\pi^+\pi^-$ mass spectrum agrees with the corresponding values calculated on CMD-2 and SND data (see Ta-

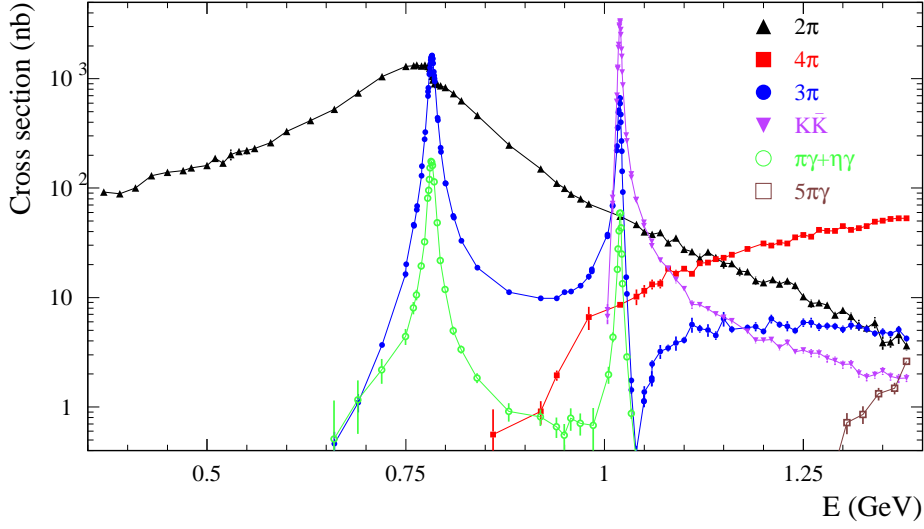


Figure 3: The hadronic cross sections measured by CMD-2 and SND detectors at VEPP-2M collider.

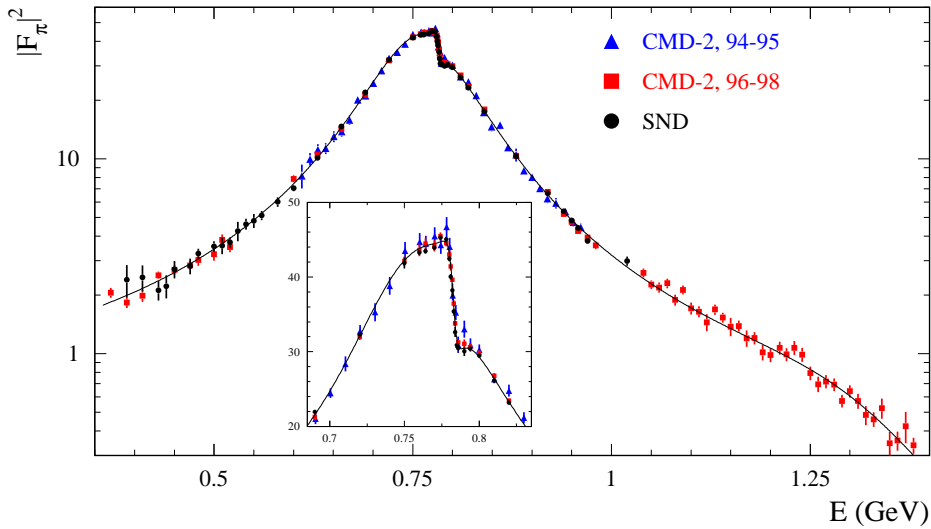


Figure 4: The pion form factor measured by CMD-2 and SND detectors. The curve is a fit result. The fit takes into account contributions of ρ , ω , and ρ' resonances.

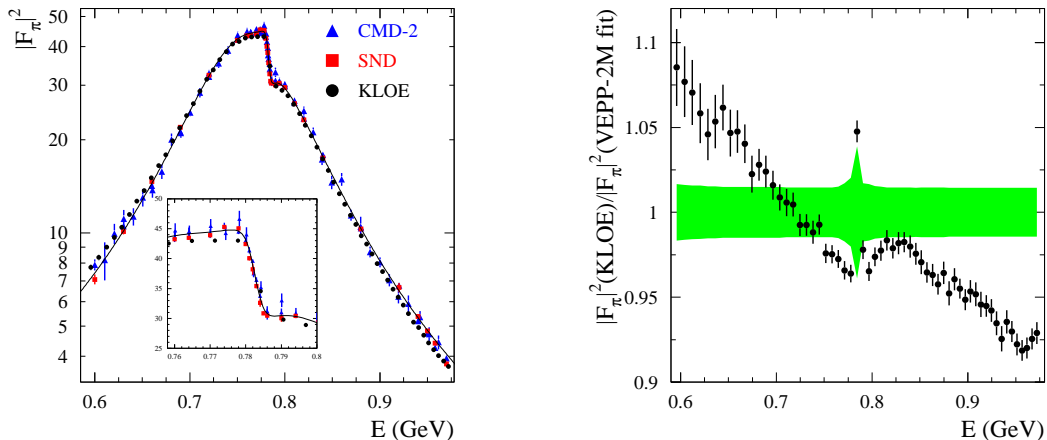


Figure 5: Left: Comparison of pion form factors measured at VEPP-2M and at KLOE. The curve is the fit to VEPP-2M data. Right: Ratio of the KLOE pion form factor to the fit to VEPP-2M data. The shaded band shows joint systematic error of the form factor measurements.

Table 2: Comparison of the 2π contributions into a_μ^{had} (in units of 10^{-10}) calculated using CMD-2, SND, and KLOE data from the energy range 0.630–0.958 GeV. The first error is statistical, the second is systematic.

experiment	$a_\mu^{\pi\pi}$
CMD-2, 94-95 [10]	$362.1 \pm 2.4 \pm 2.2$
CMD-2, 98 [11]	$361.5 \pm 1.7 \pm 2.9$
SND [14]	$361.0 \pm 2.0 \pm 4.7$
KLOE, 01 [16]	$357.2 \pm 0.5 \pm 4.6$
KLOE, 02 [17]	$355.5 \pm 0.5 \pm 3.6$

ble 2). There is, however, a significant discrepancy between the energy dependencies of pion form factors measured at VEPP-2M and in KLOE experiment (Fig.5).

Table 2 also contains the KLOE preliminary result based on statistics collected in 2002 [17]. The new software trigger, improvement in the offline background filter, and more accurate calculation of the luminosity were introduced, leading to decrease of systematic error. A bias in the evaluation on the trigger correction for the published analysis of 2001 data was found which affects at the low $\pi^+\pi^-$ mass region. The 0.7% decrease of

the predicted cross section for Bhabha scattering used for normalization, also was found. The updated 2001 $e^+e^- \rightarrow \pi^+\pi^-$ cross section and the preliminary 2002 cross section are compared in Fig. 6. In spite of nonstatistical difference between the two measurements seen near the maximum of ρ -peak, the values of $a_\mu^{\pi\pi}$ calculated over full mass region, $(384.4 \pm 0.8 \pm 4.9) \times 10^{-10}$ for 2001 data and $(386.3 \pm 0.6 \pm 3.9) \times 10^{-10}$ for 2002 data, are in good agreement. The KLOE also presents the measurement of $e^+e^- \rightarrow \pi^+\pi^-$ cross section with the ISR photon detected at large angle ($50^\circ < \theta_\gamma < 130^\circ$). In this case the threshold mass region becomes accessible. Comparison of the small angle and large angle measurements are demonstrated in Fig. 7. The systematic uncertainty for the large angle measurement is shown by the shaded band. The main source of the uncertainty is subtraction of the final state radiation background. The large angle and small angle measurements agree within the systematic errors.

The good cross check for the ISR measurement of $e^+e^- \rightarrow \pi^+\pi^-$ is simultaneous selection of $e^+e^- \rightarrow \mu^+\mu^-\gamma$ events. This allows to test ISR method using the QED process with known cross section. Taking $\pi^+\pi^-/\mu^+\mu^-$ ra-

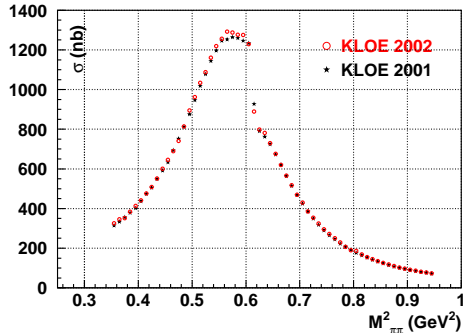


Figure 6: The $e^+e^- \rightarrow \pi^+\pi^-$ cross section measured by KLOE. The dark stars shows updated 2001 data. The preliminary 2002 data is shown by the circles.

tio reduces the systematic uncertainty, in particular, due to radiative effects. KLOE plans to measure $\pi^+\pi^-/\mu^+\mu^-$ ratio for the final result.

Other KLOE result is the measurement of the $e^+e^- \rightarrow \omega\pi^0$ cross section in the vicinity of ϕ -resonance [18]. In this region two process, nonresonant $\omega\pi^0$ production and $\phi \rightarrow \omega\pi^0$ decay, determine the total $\omega\pi^0$ cross section. The decay reveals itself as interference pattern in the cross section energy dependence. The process was studied in the two final states: $\pi^+\pi^-\pi^0\pi^0$ and $\pi^0\pi^0\gamma$. In both modes the real and imaginary parts of the relative interference amplitude were measured. The obtained interference parameters and $\phi \rightarrow \omega\pi^0$ branching fraction agree with the results of the previous SND measurement [19] but have better accuracy. From the ratio of the $e^+e^- \rightarrow \omega\pi^0$ cross sections measured in the two different final states, the ratio of the ω branching fractions was obtained: $B(\omega \rightarrow \pi^0\gamma)/B(\omega \rightarrow 3\pi) = 0.0934 \pm 0.0021$. The KLOE result has accuracy better than the world average value (0.0999 ± 0.0025) and differs from it by 2 standard deviations. The inclusion of the KLOE result into the global fit of the ω parameters will lead to growth of the ω leptonic width.

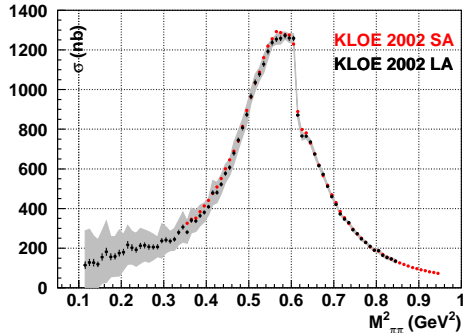


Figure 7: The $e^+e^- \rightarrow \pi^+\pi^-$ cross section measured by KLOE with the small (SA) and large (LA) angle γ selections. The shaded band indicates the systematic uncertainty for the LA measurement.

4 BABAR ISR measurements

The BABAR ISR program includes the study of all significant hadronic processes $e^+e^- \rightarrow f$ from threshold to c.m. energy about 4.5 GeV. One of the purposes of this program is measurement of R in the 1–2 GeV energy range with improved accuracy. The current status of BABAR measurements in this mass range is demonstrated in Fig. 8. To obtain the total hadronic cross section the $\pi^+\pi^-$, $\pi^+\pi^-3\pi^0$, $\pi^+\pi^-4\pi^0$, K^+K^- , $K_S K_L$, $K_S K_L \pi\pi$, $K_S K^+\pi^-\pi^0$ processes must be measured additionally. The final states $\pi^+\pi^-$, $\pi^+\pi^-3\pi^0$, K^+K^- , and $K_S K^+\pi^-\pi^0$ are currently under study. Here we discuss the latest BABAR results on $\pi^+\pi^-2\pi^0$, $2\pi^+2\pi^-\pi^0$, $2\pi^+2\pi^-\eta$, $K^+K^-\pi^0$, $K_S K^+\pi^-$, $K^+K^-\pi^+\pi^-\pi^0$ modes and measurement of strange baryon form factors.

$e^+e^- \rightarrow \pi^+\pi^-2\pi^0$. This channel is very important for calculation of a_μ^{had} and spectroscopy of the excited ρ -like states. The BABAR preliminary results on $e^+e^- \rightarrow \pi^+\pi^-2\pi^0$ cross section measurement is presented in Fig. 9. The current systematic error of the measurement varies from 8% in the cross section peak to 14% at 4.5 GeV. The comparison with existing data is shown in

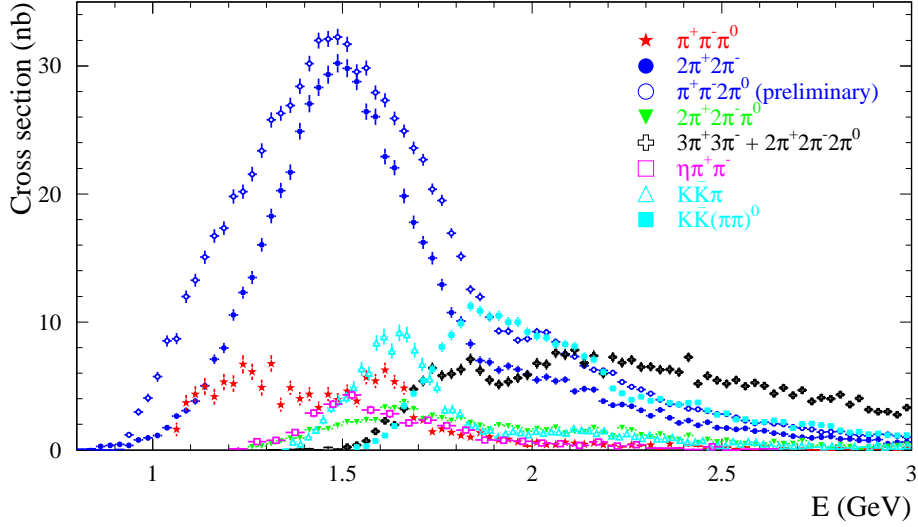


Figure 8: The hadronic cross sections measured by BABAR using ISR technique.

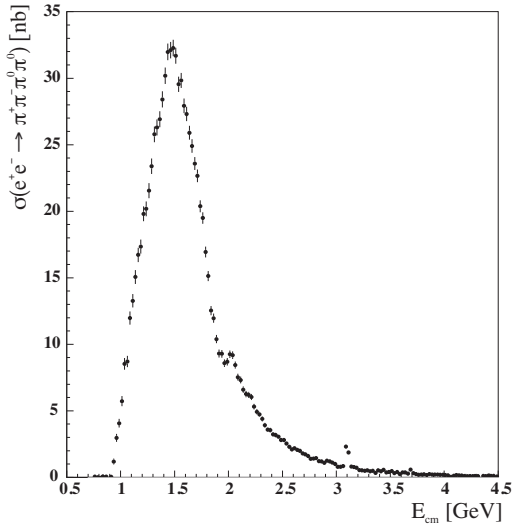


Figure 9: The $e^+e^- \rightarrow \pi^+\pi^-2\pi^0$ cross section measured by BABAR.

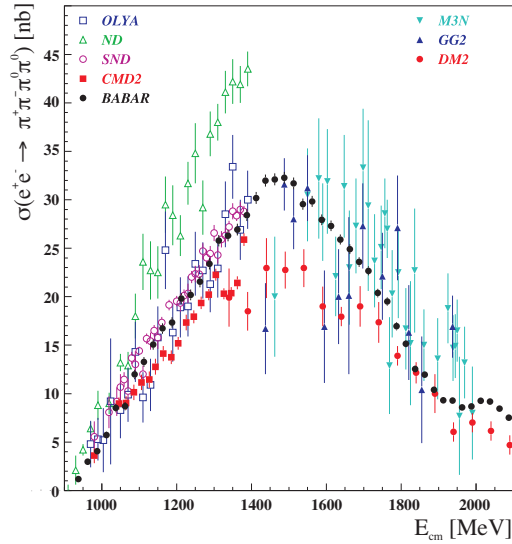


Figure 10: Comparison the BABAR data on $e^+e^- \rightarrow \pi^+\pi^-2\pi^0$ cross section with the data of other experiments.

Fig. 10. In the energy range below 1.4 GeV the the BABAR results are in good agreement with SND data. For higher energies the accuracy of the cross section is significantly improved. The BABAR data exceed the cross section measured by DM2 by about 25%. From the analysis of 3π and 2π mass distributions it was found that the $\omega\pi^0$, $a_1\pi$ and $\rho^+\rho^-$ are dominant intermediate states for $e^+e^- \rightarrow \pi^+\pi^-2\pi^0$ process. The $\rho^0 f_0(980)$ contribution is also seen. The $e^+e^- \rightarrow \rho^+\rho^-$ process was observed for the first time, its contribution was found be surprisingly large, about 30% of the total $e^+e^- \rightarrow \pi^+\pi^-2\pi^0$ cross section at $E = 1.6$ GeV.

$e^+e^- \rightarrow 2\pi^+2\pi^-\pi^0$ [20]. The measured cross section for $e^+e^- \rightarrow 2\pi^+2\pi^-\pi^0$ is shown in Fig. 8. The systematic error of the measurement is about 7%. In $\pi^+\pi^-\pi^0$ mass spectrum the ω and η peaks were observed corresponding the $\omega\pi^+\pi^-$ and $\eta\pi^+\pi^-$ intermediate states. Non- $\omega\pi^+\pi^-$ and non- $\eta\pi^+\pi^-$ events have $\rho X = \rho^0 3\pi + \rho^\pm 3\pi$ structure, where X may be $\pi(1300)$ or $a_1(1360)$. The cross sections for all three selected components were measured. The $\eta\pi^+\pi^-$ and $\omega\pi^+\pi^-$ cross sections agree with previous experiments but have significantly better accuracy. The $e^+e^- \rightarrow \eta\pi^+\pi^-$ cross section is shown in Fig. 8. A part of $\omega\pi^+\pi^-$ events contain $f_0(980)$ meson. The cross sections for the ωf_0 and non- ωf_0 components of the $\omega\pi^+\pi^-$ final state is shown in Figs. 11 and 12. The latter cross section was fitted by the sum of the contributions of ω -like resonances. From the fit, the parameters ω'' meson, $m = 1.667 \pm 0.014$ GeV and $\Gamma = 0.22 \pm 0.03$, were determined.

$e^+e^- \rightarrow 2\pi^+2\pi^-\eta$ [20]. The $2\pi^+2\pi^-\eta$ final state was studied for the first time. Three intermediate states, $\eta\rho(1450) \rightarrow \eta 4\pi$, $\eta'\rho(770)$, and $f_1(1285)\rho(770)$, were found to contribute to $2\pi^+2\pi^-\eta$. The $e^+e^- \rightarrow 2\pi^+2\pi^-\eta$ total cross section, and the cross sections for $\eta'\rho(770)$ and $f_1(1285)\rho(770)$ final states are shown in Fig. 13. The two latter cross sections are described by the single Breit-Wigner function with parameters: $m = 1.99 \pm 0.08$ GeV, $\Gamma = 0.31 \pm 0.14$

GeV for $\eta'\rho(770)$ and $m = 2.15 \pm 0.07$ GeV, $\Gamma = 0.35 \pm 0.07$ GeV for $f_1(1285)\rho(770)$. Both sets of parameters are close to those listed in the PDG tables [5] for the $\rho(2150)$.

$e^+e^- \rightarrow K^+K^-\pi^+\pi^-\pi^0$ and $K^+K^-\pi^+\pi^-\eta$ [20]. The $e^+e^- \rightarrow K^+K^-\pi^+\pi^-\pi^0$ and $e^+e^- \rightarrow K^+K^-\pi^+\pi^-\eta$ cross sections measured for the first time are shown in Fig. 14. In 3π mass spectrum for $K^+K^-\pi^+\pi^-\pi^0$ channel the η and ω peaks are observed corresponding the ωK^+K^- and $\eta\phi$ intermediate states. The cross section for $e^+e^- \rightarrow \omega K^+K^-$ is shown in Fig. 14. The $e^+e^- \rightarrow \eta\phi$ process will be discussed in the next subsection.

$e^+e^- \rightarrow K^+K^-\pi^0$, $K_S K^\pm \pi^\mp$, $\phi\pi^0$, $\phi\eta$. The $K\bar{K}\pi$ is the dominant decay mode of the $\phi(1680)$ meson. Therefore the study of $e^+e^- \rightarrow K\bar{K}\pi$ process is very important for determination of its parameters. This process was studied at BABAR in the two final states, $K^+K^-\pi^0$ and $K_S K^\pm \pi^\mp$. The measured cross sections for both channels are shown in Fig. 15. The BABAR results are in reasonable agreement with the results of the previous measurements by DM1 and DM2 but have much smaller statistical and systematic errors. The systematic uncertainty of the BABAR measurement is about 5%. Fig. 15(right) shows the Dalitz plot for $K_S K^\pm \pi^\mp$ final state. It is seen that the $KK^*(892)$ and $KK_2^*(1430)$ intermediate state give the main contributions to the $K\bar{K}\pi$ production. For $K_S K^\pm \pi^\mp$ final state both neutral $K^0 K^{*0}$ and charged $K^\pm K^{*\mp}$ intermediate states are possible. Since the $K^0 K^{*0}$ and $K^\pm K^{*\mp}$ amplitudes are the sum and the difference of the isovector and isoscalar amplitudes, the Dalitz plot population strongly depends on isospin composition. From the Dalitz plot analysis the moduli and relative phase of the isoscalar and isovector amplitudes both for $KK^*(892)$ and $KK_2^*(1430)$ final states were determined. The obtained isoscalar and isovector $e^+e^- \rightarrow KK^*(892)$ cross sections is shown in Fig. 16.

The $e^+e^- \rightarrow \phi\eta$ process was studied by BABAR in the $K^+K^-2\gamma$ and $K^+K^-3\pi$ final states. The resulted cross section is shown

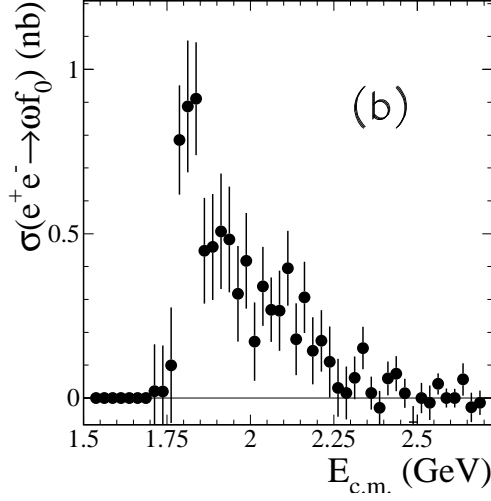


Figure 11: The $e^+e^- \rightarrow \omega f_0(980)$ cross section measured by BABAR.

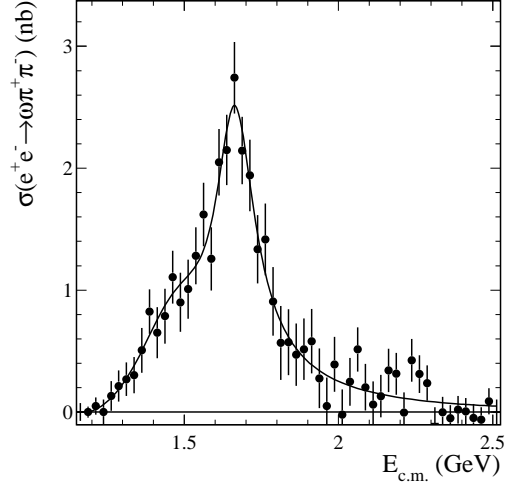


Figure 12: The $e^+e^- \rightarrow \omega \pi^+ \pi^-$ cross section with subtracted $\omega f_0(980)$ contribution. The curve is the fit result.

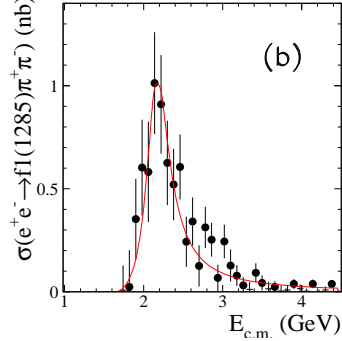
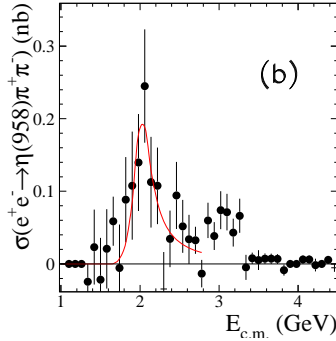
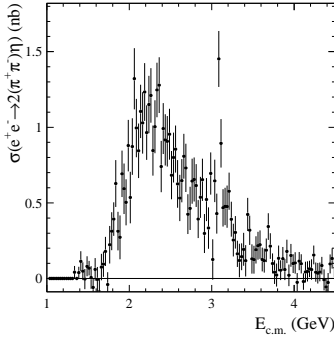


Figure 13: From left to right: The $e^+e^- \rightarrow 2\pi^+2\pi^-\eta$, $e^+e^- \rightarrow \eta'\rho(770)$ and $e^+e^- \rightarrow f_1(1285)\rho(770)$ cross sections measured by BABAR. The curves are single Breit-Wigner fits.

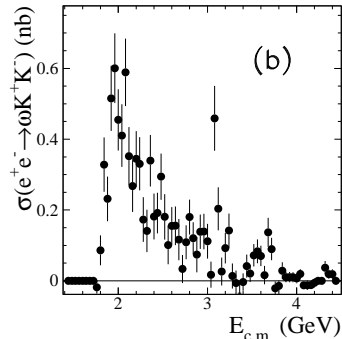
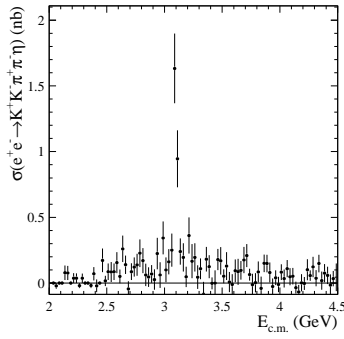
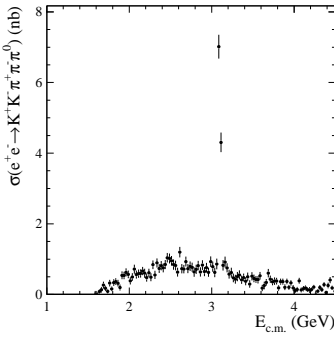


Figure 14: From left to right: The $e^+e^- \rightarrow K^+K^-\pi^+\pi^-\pi^0$, $e^+e^- \rightarrow K^+K^-\pi^+\pi^-\eta$ and $e^+e^- \rightarrow \omega K^+K^-$ cross sections measured by BABAR.

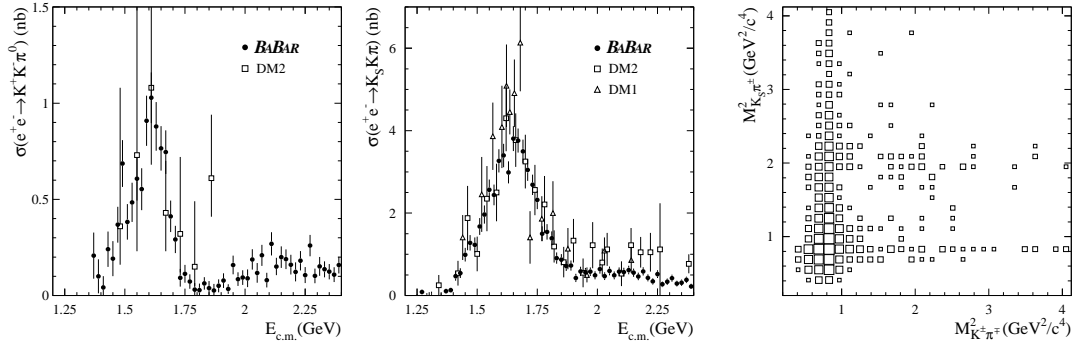


Figure 15: The $e^+e^- \rightarrow K^+K^-\pi^0$ (left) and $e^+e^- \rightarrow K_S K \pi$ (middle) cross sections measured by BABAR in comparison with results of previous measurements. Right: The Dalitz plot for $e^+e^- \rightarrow K_S K \pi$.

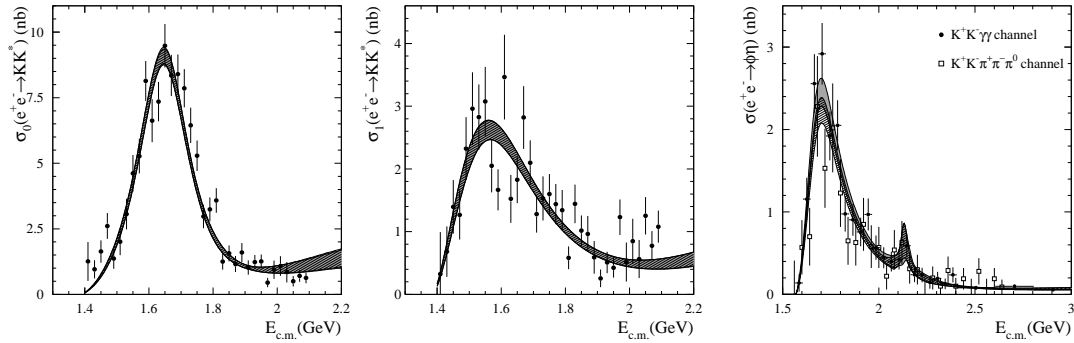


Figure 16: The isoscalar (left) and isovector (middle) $e^+e^- \rightarrow KK^*(892)$ cross sections and $e^+e^- \rightarrow \phi\eta$ (right) cross section measured by BABAR. The bands represent the fits.

in Fig. 16(right). The $e^+e^- \rightarrow \phi\eta$ is the best channel for study of excited ϕ state. The contributions of ω -like states are suppressed by OZI rule. The global fit of the $e^+e^- \rightarrow \phi\eta$ and $e^+e^- \rightarrow K^+K^-\pi^0$ cross sections, isovector and isoscalar $KK^*(892)$ amplitudes, and their relative phase was performed to determine parameters of the ϕ and ρ excitations decaying into these final states. The fit results are shown in Fig. 16. The isovector $KK^*(892)$ component is described by a single broad resonance which mass is compatible with that for $\rho(1450)$ [5]. The obtained ϕ' parameters are following: $m = 1723 \pm 24$ MeV, $\Gamma = 371 \pm 90$ MeV, $\Gamma_{ee} = 580 \pm 60$ eV, $B(\phi' \rightarrow \phi\eta)/B(\phi' \rightarrow KK^*) \approx 1/3$.

In the $\phi\eta$ cross section the peak with $m = 2139 \pm 35$ MeV and $\Gamma = 76 \pm 62$ MeV is seen with 2 sigma significance. These parameters are close to the mass and width of the state recently observed by BABAR in $\phi f_0(980)$ mode [21].

The cross section for $e^+e^- \rightarrow \phi\pi^0$ measured by BABAR in the $K^+K^-\pi^0$ final state is shown in Fig. 17. This reaction is suitable for search of exotic isovector resonances. For the ordinary isovector states, $\phi\pi^0$ decay is suppressed by OZI rule. With available limited statistics the $e^+e^- \rightarrow \phi\pi^0$ cross section is described by the single resonance with $m = 1600 \pm 30$ MeV and $\Gamma = 200 \pm 100$ MeV. These parameters are compatible with those for $\rho(1700)$ [5].

Baryon form factors [22]. BABAR continued the study of the baryon time-like electromagnetic form factors started by the work [23] on the $e^+e^- \rightarrow p\bar{p}$ reaction. The cross section for $e^+e^- \rightarrow B\bar{B}$, where B is a spin-1/2 baryon depends on two form factors, magnetic (G_M) and electric (G_E). From the measurements of the total cross section for $e^+e^- \rightarrow \Lambda\bar{\Lambda}$, $\Lambda\Sigma^0$, and $\Sigma^0\bar{\Sigma}^0$ reactions, the effective Λ , Λ - Σ^0 , and Σ^0 form factors were extracted. These form factors together with the previously measured [23] proton form factor are shown in Fig. 18. For $\Lambda\bar{\Lambda}$ channel the Λ angular distributions were studied and the ratio of the form factors was determined for the two energy regions: $|G_E/G_M| = 1.7^{+1.0}_{-0.6}$

for 2.23–2.40 GeV and $|G_E/G_M| = 0.7 \pm 0.7$ for 2.4–2.8 GeV. The obtained ratios are consistent both with $|G_E/G_M| = 1$ and with the results for $e^+e^- \rightarrow p\bar{p}$, where this ratio was found to be significantly greater than unity near threshold. The measurement of Λ polarization via its decay to $p\pi^-$ gives possibility to extract the relative phase between the electric and magnetic form factors. The limited experimental statistics allowed to set only very weak limits on this phase: $-0.76 < \sin\phi < 0.98$.

5 Tests of CVC

The hypothesis of the vector current conservation (CVC) connects the isovector e^+e^- cross section with the vector spectral function in τ decay:

$$\sigma_{e^+e^- \rightarrow X^0}^{I=1}(s) = \frac{4\pi\alpha^2}{s} v_{1,X}(s).$$

This relation holds in the limit of exact isospin invariance. Therefore the τ spectral function must be corrected for isospin-breaking effects before comparison with the corresponding e^+e^- cross section. Such corrections were considered in Ref. [24]. The pion form factor and $e^+e^- \rightarrow 4\pi$ cross sections calculated from the isospin-breaking corrected τ spectral functions are compared with the direct e^+e^- measurements in Figs. 19,20. Fig. 19 was taken from Ref. [2]. The τ 2π spectral function is obtained by averaging the ALEPH, CLEO, and OPAL data. The τ 4π spectral functions were taken from Ref. [25]. For all three reactions a significant discrepancy between e^+e^- and τ data is observed. These disagreements are difficult to explain by unaccounted isospin breaking effects. New precise τ data are needed to confirm the observed discrepancies.

6 Summary

The significant progress has been reached in the measurements of the low energy hadronic e^+e^- cross sections in last few years, leading

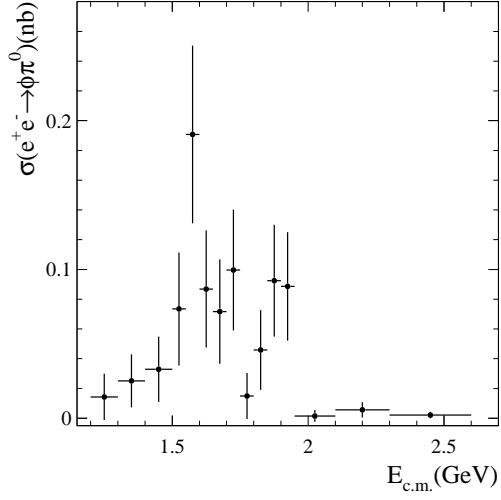


Figure 17: The $e^+e^- \rightarrow \phi\pi^0$ cross section measured by BABAR.

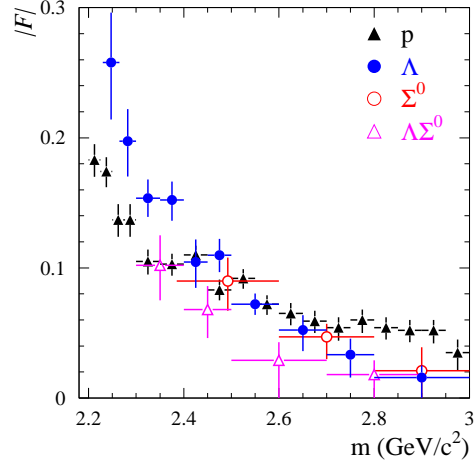


Figure 18: The octet baryon form factors measured by BABAR.

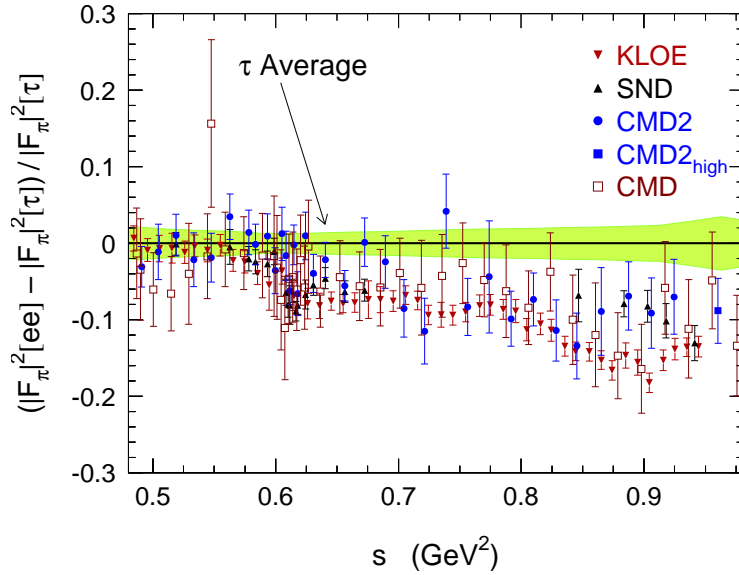


Figure 19: Comparison of the pion form factors obtained from e^+e^- -annihilation and from τ data. The shaded band indicates the errors of τ data.

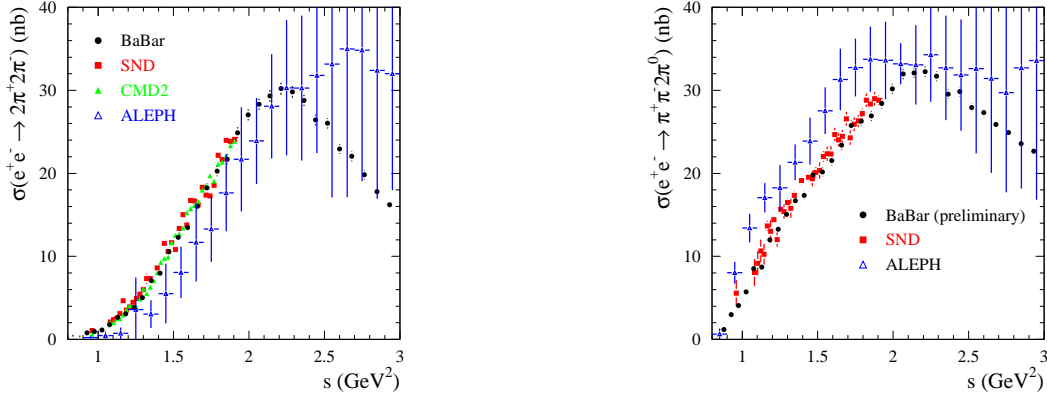


Figure 20: Comparison of $e^+e^- \rightarrow 2\pi^+2\pi^-$ (left) and $e^+e^- \rightarrow \pi^+\pi^-2\pi^0$ cross section measured in e^+e^- collisions with the cross sections calculated from the spectral functions of $\tau \rightarrow 4\pi\nu_\tau$ decays.

to improvement of the accuracy of the total hadronic e^+e^- cross section. In particular, using the recent CMD-2, SND, KLOE, and BABAR data reduces the error of the a_μ^{had} from about 7×10^{-10} in 2003 to about 4×10^{-10} in 2007. This error is now comparable with the error of the light-by-light scattering contribution, also 4×10^{-10} [26].

There are, however, the discrepancy between the energy dependencies of the pion form factors measured directly in e^+e^- collisions at VEPP-2M and via ISR at KLOE. The new ISR data on $e^+e^- \rightarrow \pi^+\pi^-$ are expected from the KLOE and BABAR. Both experiments plan to measure $\pi\pi/\mu\mu$ ratio. This will reduce the systematic error, in particular, due to radiative effects.

The new precise data on multihadron cross sections for the energy region from 1 to 3 GeV obtained at VEPP-2M and in BABAR experiment allows to improve our knowledge of the properties of the ρ , ω , and ϕ excitations. All major isoscalar channels (3π , $\omega\pi\pi$, $\omega\eta$, KK^* , $\phi\eta$) have been measured. Some theoretical input is needed to perform a global fit to the measured cross sections and extract a complete set of parameters of the isoscalar resonances. The many isovector cross sections ($2\pi^+2\pi^-$, $K^+K^-\pi\pi$, $\eta\rho$, KK^*) are also measured. The final BABAR result on $e^+e^- \rightarrow$

$\pi^+\pi^-2\pi^0$ is expected soon.

The discrepancy between the e^+e^- and isospin-breaking corrected data τ data is observed for 2π and 4π final states. This discrepancy is difficult to explain by unaccounted isospin breaking effects. New data on $\tau \rightarrow 2\pi\nu_\tau$ and $\tau \rightarrow 4\pi\nu_\tau$ decays from B factories, and ISR data on 2π channel from KLOE and BABAR should provide a test the existing e^+e^- and τ measurements.

References

- [1] G. W. Bennett *et al.* [Muon G-2 Collaboration], Phys. Rev. D **73**, 072003 (2006) [arXiv:hep-ex/0602035].
- [2] M. Davier, Nucl. Phys. Proc. Suppl. **169**, 288 (2007) [arXiv:hep-ph/0701163].
- [3] F. Jegerlehner, arXiv:hep-ph/0703125.
- [4] K. Hagiwara, A. D. Martin, D. Nomura and T. Teubner, Phys. Lett. B **649**, 173 (2007) [arXiv:hep-ph/0611102].
- [5] W.-M. Yao *et al.* [Particle Data Group], J. Phys. G **33**, 1 (2006).
- [6] J. Z. Bai *et al.* [BES Collaboration], Phys. Rev. Lett. **88**, 101802 (2002) [arXiv:hep-ex/0102003].

- [7] G. Bonneau and F. Martin, Nucl. Phys. B **27**, 381 (1971).
- [8] M. N. Achasov *et al.* [SND Collaboration], arXiv:0707.2279 [hep-ex].
- [9] M. N. Achasov *et al.* [SND Collaboration], arXiv:0709.1007 [hep-ex].
- [10] R. R. Akhmetshin *et al.* [CMD-2 Collaboration], Phys. Lett. B **578**, 285 (2004) [arXiv:hep-ex/0308008].
- [11] R. R. Akhmetshin *et al.* [CMD-2 Collaboration], Phys. Lett. B **648**, 28 (2007) [arXiv:hep-ex/0610021].
- [12] R. R. Akhmetshin *et al.* [CMD-2 Collaboration], JETP Lett. **84**, 413 (2006) [Pisma Zh. Eksp. Teor. Fiz. **84**, 491 (2006)] [arXiv:hep-ex/0610016].
- [13] V. M. Aulchenko *et al.* [CMD-2 Collaboration], JETP Lett. **82**, 743 (2005) [Pisma Zh. Eksp. Teor. Fiz. **82**, 841 (2005)] [arXiv:hep-ex/0603021].
- [14] M. N. Achasov *et al.* [SND Collaboration], J. Exp. Theor. Phys. **103**, 380 (2006) [Zh. Eksp. Teor. Fiz. **130**, 437 (2006)] [arXiv:hep-ex/0605013].
- [15] M. N. Achasov *et al.* [SND Collaboration], Phys. Lett. B **474**, 188 (2000) [arXiv:hep-ex/0001048].
- [16] A. Aloisio *et al.* [KLOE Collaboration], Phys. Lett. B **606**, 12 (2005) [arXiv:hep-ex/0407048].
- [17] F. Ambrosino *et al.* [KLOE Collaboration], arXiv:0707.4078 [hep-ex].
- [18] F. Ambrosino *et al.* [KLOE collaboration], arXiv:0707.4130 [hep-ex].
- [19] V. M. Aulchenko *et al.*, J. Exp. Theor. Phys. **90** (2000) 927 [Zh. Eksp. Teor. Fiz. **90** (2000) 1067].
- [20] B. Aubert *et al.* [BABAR Collaboration], arXiv:0708.2461 [hep-ex].
- [21] B. Aubert *et al.* [BABAR Collaboration], Phys. Rev. D **74**, 091103 (2006) [arXiv:hep-ex/0610018].
- [22] B. Aubert *et al.* [BABAR Collaboration], arXiv:0709.1988 [hep-ex].
- [23] B. Aubert *et al.* [BABAR Collaboration], Phys. Rev. D **73**, 012005 (2006) [arXiv:hep-ex/0512023].
- [24] V. Cirigliano, G. Ecker and H. Neufeld, JHEP **0208**, 002 (2002) [arXiv:hep-ph/0207310].
- [25] S. Schael *et al.* [ALEPH Collaboration], Phys. Rept. **421**, 191 (2005) [arXiv:hep-ex/0506072].
- [26] J. Bijnens and J. Prades, Mod. Phys. Lett. A **22**, 767 (2007) [arXiv:hep-ph/0702170].